 FDMP, vol.2, no.4, pp.287-295, 2006

The Influence of Flow Pressure Gradient on Interfacial Wave Properties in Annular Two-Phase Flow at Microgravity and Normal Gravity Conditions

Huawei Han[1] **and Kamiel S. Gabriel**[2]

Abstract: In earlier experimental studies data on air-water co-current two-phase annular flow in a tube with an inner diameter of 9.525 mm (3/8 in) were collected at both microgravity (μ-g) and normal gravity (1-g) conditions. The data contained measurements of pressure drop, in addition to previously published data of liquid film thickness. This paper presents a critical review of such results. In particular, a rich analysis of the influence of flow pressure gradient on interfacial wave properties of the annular flow is carried out. The examined wave properties include wave base thickness, wave height (or roughness height), wave spacing, wave speed and wave frequency. It is shown that, the average liquid film thickness, wave base thickness, wave height, and wave spacing decrease with increase of the pressure gradient at both gravity levels; whereas, the wave speed and wave frequency linearly increase regardless of the gravity level. Comparison of the wave properties under 1-g and μ-g conditions highlights that the average liquid film thickness at μ-g is 2 to 3 times as thick as that at 1-g; the wave base thickness at μ-g is $2 \sim 4$ times as thick as that at 1-g; the wave height or roughness height at μ-g is 50% less than that at 1-g; and the wave spacing at μ-g is 3 to 4 times as long as its counterpart at 1-g. Relevant interpretations of these results are also included in the paper.

keyword: Pressure gradient, Wave properties, Annular flow, Microgravity, Normal gravity.

1 Introduction

Gas-liquid two-phase annular flow frequently occurs in thermal management and thermal control systems of terrestrial energy transport systems, such as flow channels of nuclear reactors, boilers, and heating and refrigeration equipment. This type of flow is characterized by a liquid film flowing on the inner tube wall, a gas core flowing in the center of the tube, and a rough gas-liquid interface covered by highly dynamic waves. Extensive studies indicate that large disturbance waves travel on the gas-liquid interface with smaller-amplitude ripple waves and it is commonly believed that the disturbance waves more significantly influence two-phase flow behaviors (such as mass, momentum and energy transfer between the two phases) than ripple waves.

Annular flow has been the subject of extensive studies during the past three decades including pressure drop prediction using empirical or semi-empirical relations. However, in reviewing the literature, it is apparent that while pressure-drop predictions in single phase flow have been well developed; it is not the case for two-phase annular flow. This is mainly due to the complicated flow structures, the difficulty in taking in-situ measurements without influencing the flow regime, and in general the lack of cohesive data that includes all flow parameters. Presently, the literature contains numerous empirical correlations capable of predicting the two-phase pressure drop or friction factor within 25-50%.

Due to the significant role of waves and in order to better predict the frictional pressure-drop in two-phase flow, the flow interface structure was extensively studied. For example, Wang and coworkers (2005 & 2004) used a large set of experimental data (also used in this study) to predict the interfacial friction factor and relative interfacial roughness (wave height) of air-water annular flow in a small diameter tube (9.525 mm i.d.). Data were taken at different gravitational fields allowing for isolating the effect of gravity on the flow structure. In their studies, the roughness height (wave height) on the two-phase interface was considered the relative interfacial roughness and the interfacial friction factor was analytically derived from force balance in the annular flow. Results at microgravity and normal gravity were presented and showed that the wave height and relative interfacial roughness at microgravity were less than half of the corresponding values at normal gravity; and the interfacial fric-

[1] PostDoc. Fellow, Faculty of Engineering & Applied Science, University of Ontario Institute of Technology, Oshawa, ON, CA.

[2] Associate Provost, Research, University of Ontario Institute of Technology, Oshawa, ON, CA.

tion factor in annular flow increased with increasing the interfacial roughness and decreased with increasing the gas Reynolds number. Wrobel and McManus (1961) predicted the pressure drop in annular flow by directly correlating the friction factor with the interfacial roughness. Also, Henstock and Hanratty (1976) and Asali *et al.* (1985) studied the relationship between the pressure drop and the liquid film height for gas-liquid annular flow and they directly correlated the interfacial drag with the liquid film height based on their flow measurements. An earlier work to establish a relationship between the pressure drop and the wave spacing was presented by Moalem Maron and Brauner (1987) in which they suggested that the pressure drop was directly related to the waviness of the film and the mobility of the interface.

It could be concluded from the above studies that earlier efforts focused on correlating the pressure drop or the friction factor with one or two parameters of the interfacial wave structure with the intention to obtain a reliable pressure drop estimation of the flow. However, just as Moalem Maron and Brauner (1987) suggested, the pressure drop is related not only to the wave structure but also to other hydrodynamics features of the waves. Hence, the study of the relationship between the pressure drop and the interfacial waves should be a more holistic one. In essence, not only the wave structure's influence should be considered, but also its dynamic properties. This paper is intended to present for the first time a comprehensive approach to establish the relationship between pressure drop and wave characteristics in gas-liquid two-phase flows.

The literature contains a very limited data set that links pressure drop and interfacial wave for microgravity annular flow. Chen *et al.* (1991) presented their experimental data of two-phase annular flow pressure drop in normal gravity and at near zero-gravity condition aboard a NASA-JSC KC-135 aircraft. Based on that limited data set, an annular flow model with an interfacial friction factor was developed from the near zero-gravity data. Bousman and coworkers (1993 & 1996) measured pressure drop at microgravity condition and also developed a model for the prediction of pressure drop at microgravity. It was also reported that during their experiments, the liquid film thickness data at microgravity condition was obtained; but regrettably, such data was not used to further develop wave information. Fujij et al. (1998) measured the pressure drop and liquid film thickness of gaseous nitrogen (GN_2)-water annular flow at microgravity condition in a 10-s drop tower. Based on the liquid film thickness data the interfacial roughness (wave height) was compared to its counterpart at normal gravity with no conclusive results given the very limited data set and short duration of microgravity.

In the present study, a comprehensive data set that includes pressure drop and wave properties (wave structure and wave speed) is used to develop a relationship between the pressure drop and the interfacial wave properties at both normal gravity and microgravity conditions. Hence the influence of the pressure gradient on the interfacial wave properties in air-water co-current two-phase annular flow could be more accurately predicted. In addition, the wave properties at both gravity levels are also presented and discussed.

2 Instrumentation and data analysis

The data used in this study were collected by MacGillivray (2002 & 2003) for air-water annular flow at microgravity (μ-g) and normal gravity (1-g) conditions. The co-current two-phase annular flow was developed in a vertical tube with an inner diameter of 9.525 mm (3/8 in). The microgravity data were obtained aboard a Zero-gravity Airbus A300 (operated by Novespace out of Bordeaux, France) during two Microgravity Science missions of the European Space Agency. Microgravity in this case refers to the conditions where the gravitational acceleration on the aircraft is in the range of +/- 0.05 of earth gravity (normal gravity). The normal gravity data were collected using the same experimental loop on the ground. The main independent parameters measured and recorded in these data sets are the liquid and gas mass flow rates, void fraction, the liquid film thickness, and the two-phase pressure drop across the test section. Data were collected at a sampling rate of 1024 Hz. The pressure drop was measured using a +/-2 psi differential (diaphragm type) pressure transducer. The liquid film thickness was measured using two parallel wire conductance probes. The data were then processed to obtain the average pressure gradient, the interfacial wave structure and wave speed. Uncertainties of the most important two flow parameters measured were calculated: the maximum uncertainty for liquid film thickness measurements is 0.104 mm and the counterpart for pressure drop is 353 Pa. For further details on the design, experimental loop, calibration, measurement procedure, instrumentation and

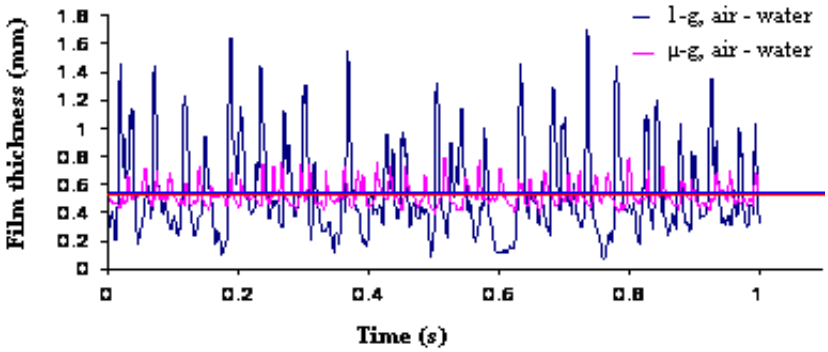

Figure 1 : A sample of time trace of the liquid film thickness at different gravity levels.

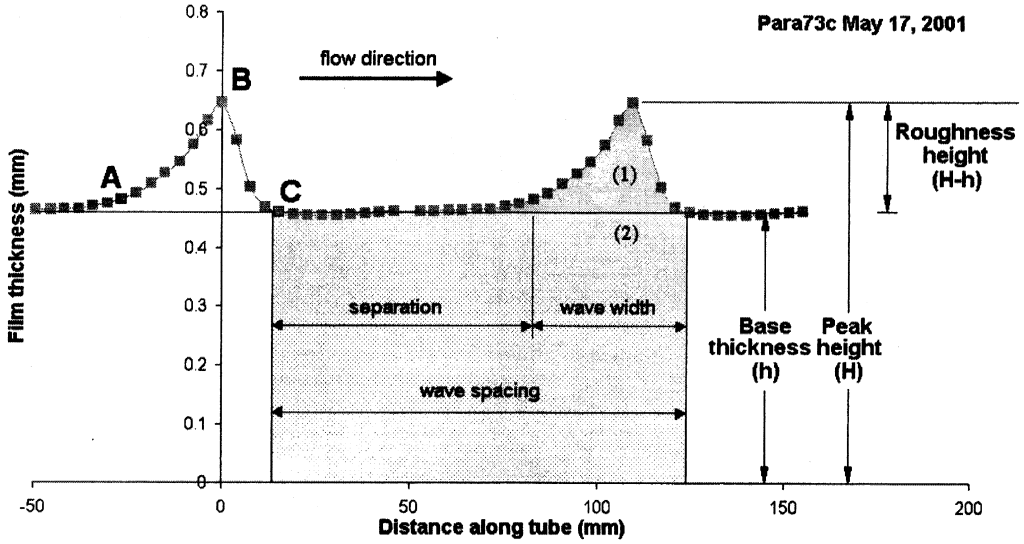

Figure 2 : A sample wave shape; Han *et al.* (2006).

uncertainty analysis, the reader is referred to the work of MacGillivray (2002, 2003 and 2004).

In the experiments, the time trace of the liquid film thickness for each of the set points was recorded. Figure 1 shows the liquid film thickness time trace of the flow measured at both microgravity and normal gravity conditions. It can be seen that the time trace features a series of wave peaks and valleys that are much less obvious in microgravity; indicating that reduced gravity has a "suppressive" effect on the two-phase interface. A wave shape was obtained using the recorded time trace. The local wave peaks in the time trace were identified using the cutoff criterion developed earlier by De Jong (2003); defined as the sum of the average film thickness plus one standard deviation of the film thickness. The wave speed was determined using the cross spectral density (CSD) technique. Flow map analysis by Zhu (2004) indicated that the waves obtained in this study were disturbance waves. Figure 2 shows a sample wave shape. More details on the wave profile development and the definitions of the wave nomenclatures, such as wave spacing, wave base thickness (film substrate), and wave height (roughness height), can be found in the work by Wang et al. (2004) and Han et al. (2006). Han et al. (2006) also presented detailed characteristics of the disturbance waves in their work.

3 Pressure drop results and discussions

In this section, the pressure gradient results at both microgravity and normal gravity conditions are presented and discussed in terms of their influence on the wave characteristics. The experimental conditions were such that the liquid superficial velocity ranged from 0.1 to 0.2 m/s (0.00540 $\sim$ 0.01173 kg/s), the gas superficial veloc-

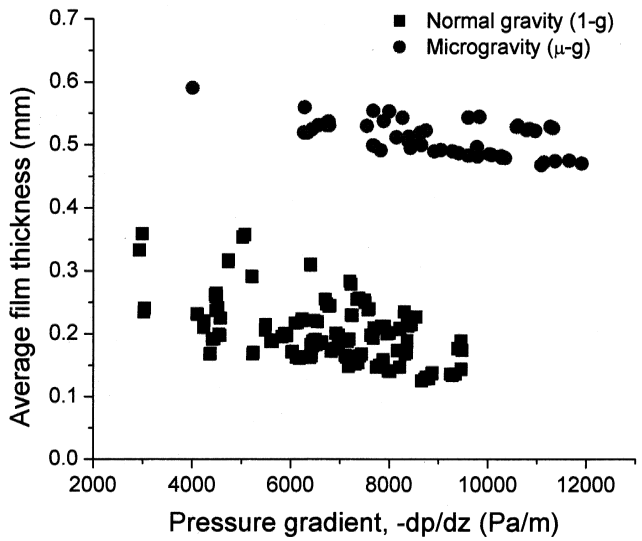

Figure 3 : Influence of pressure gradient on the average film thickness at both microgravity and normal gravity.

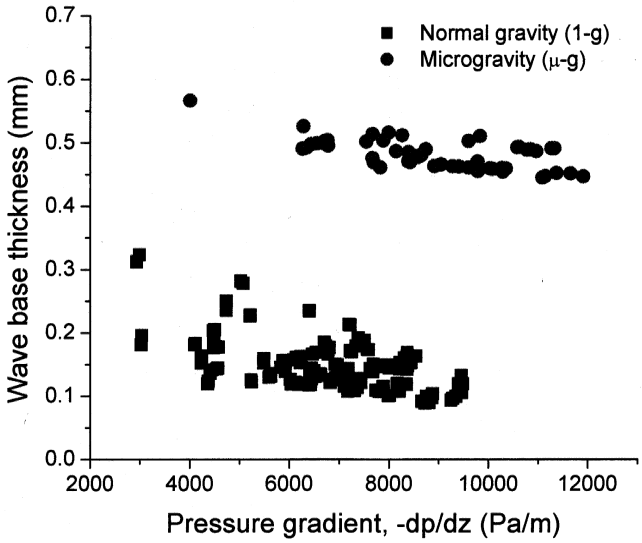

Figure 4 : Influence of pressure gradient on wave base thickness at both microgravity and normal gravity.

ity ranged from 16 to 40 m/s (0.00102 $\sim$ 0.00340 kg/s) at atmospheric pressure. The corresponding pressure gradient in this range varied from 2900 Pa/m to 12000 Pa/m. The wave parameters include the wave base thickness (film substrate), wave height (roughness height), wave spacing, wave frequency and wave speed. For interested readers, these data are tabulated in Appendix A.

3.1 Relationship with the average liquid film thickness

Because wave properties were drawn from the information of liquid film thickness and in order to better understand relationship between pressure drop and the interfacial wave properties, the relationship between the pressure drop and average liquid film thickness were presented first. Figure 3 shows the relationship between the pressure gradient and the average liquid film thickness at both microgravity and normal gravity conditions. These results suggest that the average liquid film thickness slightly decreases with the increase of the pressure gradient at both 1-g and μ-g conditions. While in single liquid-phase flow, the increase in pressure gradient is a result of increasing the liquid flow rate, this is not necessarily the case in two-phase flow. Increasing the gas-phase flow rate at a constant liquid mass flow rate could lead to an increase in the liquid entrainment rate; typically accompanied by an increase in the pressure gradient. Higher entrainment rates resulting from increasing the gas flow rate, and hence the pressure gradient, could then lead to a decrease in the average liquid film thickness. This is the case in the present experiments. The above discussions are based on the work of Han et al. (2005), who measured liquid entrainment fraction on the ground at the same experimental conditions as those in this study.

It is impressive to note from Figure 3 that the average liquid film thickness at microgravity condition is 2 to 3 times as thick as that at normal gravity. This shows a significant influence of gravitational force on the liquid film structure. For air-water upward co-current annular flow, gravity acts as an "obstruction" force. When gravity is reduced, for the same pressure gradient, more liquid and gas are pushed into the flow loop. Also, due to the compressibility of the gas phase, the above mentioned result was obtained. One point is noted here that the average liquid film thickness could be viewed as the height when a smooth two-phase interface is assumed.

3.2 Relationship with the wave base thickness (film substrate)

Figure 4 presents the results of the pressure gradient and the wave base thickness at both 1-g and μ-g conditions. It could be inferred from the figure that the wave base thickness at microgravity condition is 2 $\sim$ 4 times as thick as that at normal gravity. It can be seen that the pressure

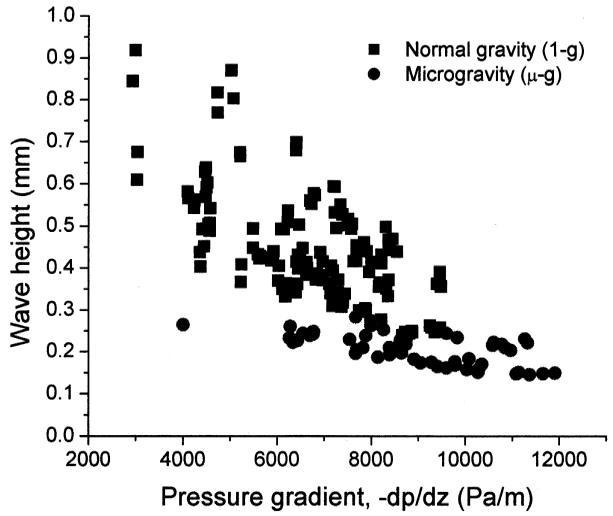

Figure 5 : Influence of pressure gradient on wave height (roughness height) at both microgravity and normal gravity.

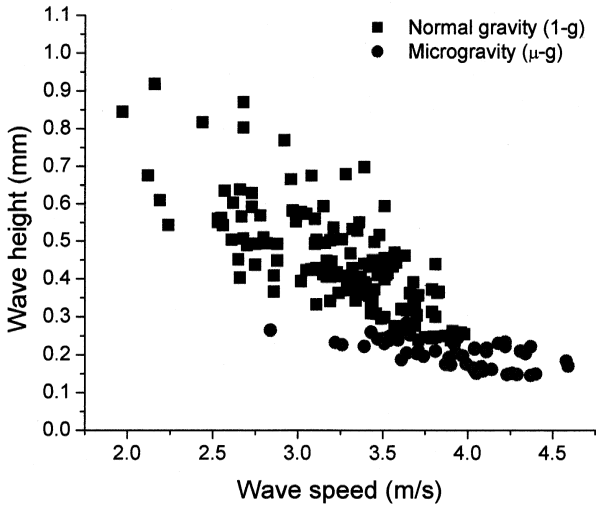

Figure 6 : Influence of wave speed on wave height (roughness height) at both microgravity and normal gravity.

gradient exerts similar influence on the wave base thickness as that on the average film thickness, which may be attributed to the same effect as that resulting in the decrease of the average liquid film thickness.

Owing to the formation of interfacial waves on the two-phase interface, the liquid portion in the film is redistributed. Hence, the wave base thickness is reduced compared to the average liquid film thickness at both microgravity and normal gravity. When we compare the results of Figure 4 with those shown earlier in Figure 3, it can be seen that the reduction in the film thickness at both gravity levels is not significant, which suggests that only a small portion of the liquid phase goes into the interfacial waves. Further detailed comparison indicates that the extent of the film thickness reduction, whether relative or absolute, at microgravity is significantly less than that at normal gravity, which suggests that less liquid phase is redistributed into the interfacial waves at microgravity. This phenomenon is due to larger wave height and more induced waves on two-phase interface of air-water annular flow at normal gravity condition. Such results will be discussed and analyzed in sections 3.3 & 3.5 respectively.

3.3 Relationship with the wave height (roughness height)

As with the above analysis of film substrate thickness and the average film thickness, it is mentioned that the wave height at microgravity is orders of magnitude less than that at normal gravity. This can be seen from Figure 5. It demonstrates that wave height at microgravity is 50% less than that at normal gravity at the same pressure gradient. Some researchers (Benjamin, 1957 and Clark et al. 1998) attributed this change to the enhancement of gravity in the formation of the waves and thus the interfacial waves have greater amplitudes at normal gravity than those at microgravity.

It can be seen that with the increase of the pressure gradient, the wave height or interfacial roughness height decreases. This can be interpreted by the "suppression" effect discussed earlier and also reported by Asali and Hanratty, 1993; and Nedderman and Shearer, 1963. This phenomenon is mainly due to an increase of the gas phase flow rate. From Figure 4, we can see a similar trend of the wave base thickness to that seen earlier with the wave height. As the pressure gradient or the gas flow rate increases, more water moves to the core. Hence, we can conclude that this "suppression" effect is actually the result of liquid phase entrainment into the gas core since the principal liquid entrainment mechanism in annular flow is commonly interpreted as wave peak shearing-off by incoming gas phase.

This also explains why in Figure 5 the higher the wave height at lower pressure gradient (or gas flow rate) under normal gravity condition, the larger is the suppression effect. Within the phase flow rate range in this study, at

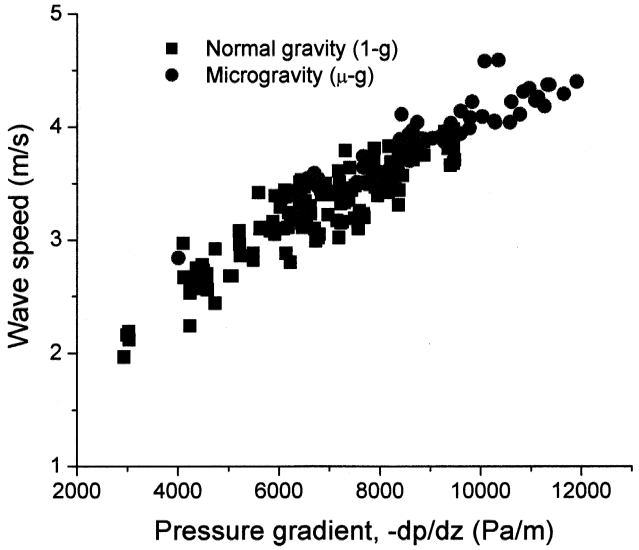

Figure 7 : Influence of pressure gradient on wave speed at both microgravity and normal gravity.

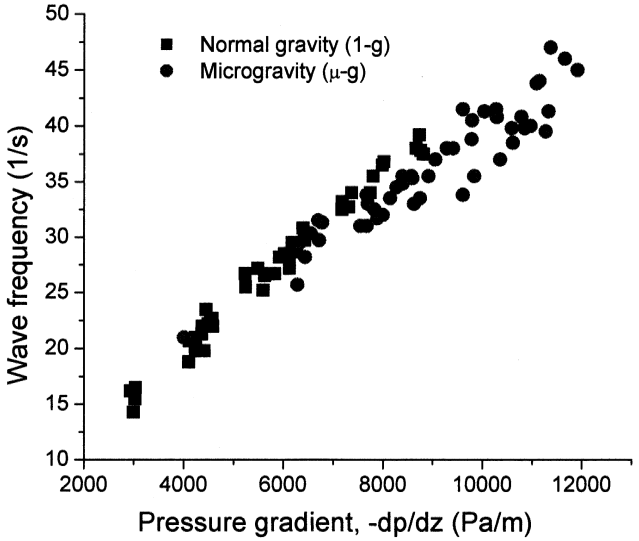

Figure 8 : Influence of pressure gradient on wave frequency at both microgravity and normal gravity.

normal gravity wave entrainment mechanism dominates in annular flow and wave peak region is significantly sheared into the gas core with the increase in the gas phase flow rate. While at microgravity condition, waves are not developed well enough to trigger extensive liquid entrainment. Hence, it is shown in Figure 5 that the wave height seems little influenced by the increase in the pressure gradient or gas flow rate.

Figure 6 shows the relationship between the wave speed and wave height (roughness height). Comparing Figure 6 with Figure 5, it seems that the wave speed has the same effect on the wave height as that of the pressure gradient. Hence, it is concluded that this figure actually represents a very interesting relationship between the pressure gradient and wave speed, which is shown in Figure 7.

3.4 Relationship with the wave speed and wave frequency

Figure 7 shows the influence of the pressure gradient on the wave speed. In both cases (microgravity and normal gravity), it can be seen that the wave speed linearly increases with the increase of the pressure gradient. This could be attributed to the increased interfacial drag acting on the interfacial waves due to the increase in the pressure gradient. It is interesting to note that this linear trend of wave speed appears to be not much influenced by changing the gravity levels. Thereby, a correlation is provided here for the wave speed in the range of pressure gradient used in the experiments:

$$V_w = 2.46 \times 10^{-4}(-dp/dz) + 1.59 \tag{1}$$

where, V_w is the interfacial wave speed (m/s); and dp/dz is the pressure gradient (Pa/m).

To explain the results shown above, one must understand the dominant role of the interfacial drag in determining the dynamic properties of interfacial wave in upward co-current annular flow since it is the only dynamic force directly acting on the wave body. To further explain this, consider a control volume in the gas core. From force equilibrium, the following relation is easily determined:

$$-\frac{dp}{dz} = \frac{4\tau}{d} + \rho g \tag{2}$$

where, d is diameter of gas core in annular flow (m); τ, the interfacial drag stress (Pa); and ρ is density of gas phase or mixture (gas phase & liquid droplets; kg/m^3). Comparing the magnitude of the pressure and gravitational forces terms in Equation (2), the latter term can be neglected whether it is under microgravity or normal gravity condition. Hence, we have:

$$-\frac{dp}{dz} = \frac{4\tau}{d} \tag{3}$$

Therefore, in this study the relationship between the pressure gradient and the wave speed are little influenced by changing the gravity level.

The relationship between the pressure gradient and wave frequency, Figure 8, shows the same trend since the relationship between the wave speed and wave frequency is a linear one. The influence of pressure gradient on the wave frequency is very similar to that for the wave speed at both gravity levels.

3.5 Relationship with the wave spacing

Figure 9 shows the relationship between the pressure gradient and the wave spacing at both 1-g and μ-g conditions. The wave spacing at microgravity is 3 to 4 times as large as its counterpart at normal gravity. In the other words, the wave density on the two-phase interface at normal gravity is 3 to 4 times as dense as that at microgravity. Referring back to previous results where it was shown that the wave height at microgravity is less half than that at normal gravity, it is concluded that the interface in two-phase annular flow at microgravity is much smoother than that at normal gravity. As mentioned previously, this is also the reason why the reduction in the film thickness at normal gravity is much more prevalent than that at microgravity. These results clearly demonstrate that gravity plays an important role in inducing and enhancing the wave formation on the two-phase interface of the air-water annular flow.

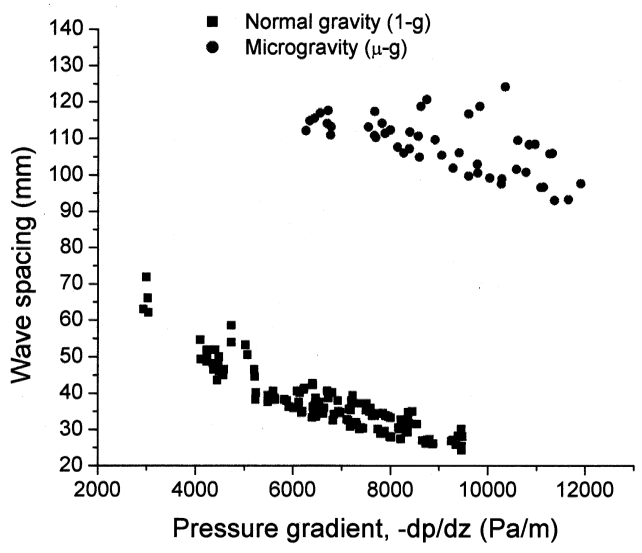

Figure 9 : Influence of pressure gradient on wave spacing at both microgravity and normal gravity.

From Figure 9, it can be also seen that with the increase in the pressure gradient, the wave spacing decreases at both normal and microgravity conditions. This means that more interfacial waves were generated on the two-phase interface as a result of increasing the pressure gradient. It is known that with the increase in the pressure gradient, the interfacial drag increases, which in return could induce the generation of more waves on the interface and hence reduce the wave spacing for each wave.

4 Conclusions

1. Average liquid film thickness at μ-g is 2 to 3 times as thick as that at 1-g. It illustrates the significant influence of gravitational acceleration on the liquid film in annular flow. It is mainly attributed to the removal of flow obstruction at microgravity and compressible property of gas phase. At both gravity levels, with the increase of the pressure gradient the average liquid film thickness respectively decreases. This is attributed to the more liquid entrainment into the gas core due to the increase of pressure gradient.

2. The wave base thickness at μ-g is $2 \sim 4$ times as thick as that at 1-g. It also indicates a significant influence of gravity on the wave structure. It is attributed to the various liquid redistribution capabilities of the interfacial waves at different gravity levels. With the increase of the pressure gradient, the wave base thickness decreases at both 1-g and μ-g conditions, which may be attributed to the same reason as the decrease of the average liquid film thickness.

3. The wave height (or roughness height) at μ-g is 50% less than that at 1-g. This is attributed to the wave-enhancement ability of gravity. At both gravity levels, with the increase of the pressure gradient, the wave height or interfacial roughness height decreases. This is attributed to the "suppression" effect of the increased gas velocity due to the increase in the pressure gradient.

4. The wave speed and wave frequency linearly increase with the increase in the pressure gradient at both μ-g and 1-g conditions. Their respective increasing trends seem not influenced by changing the gravity level. This is interpreted that dynamic properties of the interfacial wave are determined by the

interfacial drag, which is only determined by the pressure gradient at both microgravity and normal gravity conditions in the studied annular flow. The increase of the wave speed with that of the pressure gradient is explained as the increase of the interfacial drag acting on the waves in the flow; and a correlation was presented to describe the linear relationship between the pressure gradient and the wave speed.

5. The wave spacing at μ-g is 3 or 4 times as long as its counterpart at 1-g (in conjunction with the much smaller wave height at μ-g), which makes the two-phase interface of annular flow at μ-g much smoother. This phenomenon is attributed to the strong wave-inducement role of gravity. Wave spacing decreases with the increase of the pressure gradient at both μ-g and 1-g conditions. This may be attributed to the strengthened wave-inducement ability of increased interfacial drag due to the increase of pressure gradient.

References

Asali, J.C.; Hanratty, T.J. (1993): Ripples generated on a liquid film at high gas velocities. *International Journal of Multiphase Flow*. Vol.19, pp. 229-243.

Asali, J. C.; Hanratty, T. J. and Andreussi, P. (1985): Interfacial Drag and Film Height for Vertical Annular Flow. *AIChE Journal*, Vol. 31, pp. 895-902.

Benjamin, T.B. (1957): Wave formation in laminar flow down an inclined plane, *Journal of Fluid Mechanics.* Vol. 2, pp. 554-574.

Bousman, W.S. (1993): Studies of gas-liquid flow in microgravity: void fraction, pressure drop and flow patterns. *American Society of Mechanical Engineers, Applied Mechanics Division, AMD,* Vol. 174, *Fluid Mechanics Phenomena in Microgravity,* pp. 23-36.

Bousman, W.S.; McQuillen, J.B. and Witte, L.C. (1996): Gas-liquid flow patterns in microgravity: effects of tube diameter, liquid viscosity and surface tension. *International Journal of Multiphase Flow,* Vol. 22, pp. 1035-1053.

Chen, I.; Downing, R.; Keshock, E. G. and Al-Sharif, M. (1991): Measurements and Correlation of Two-phase Pressure Drop under Microgravity Condition. *Journal of Thermophysics and Heat Transfer,* Vol. 5, pp. 514-523.

Clark, W.W.; Hills, J.H. and Azzopardi, B.J. (1998): The interfacial characteristics of falling film reactors. In: *Proceedings presented at the IChemE Research Event*, NewCastle.

De Jong, P.; Gabriel, K.S. (2003): A Preliminary Study of Two-Phase Annular Flow at Microgravity; Experimental Data of Film Thickness, *International Journal of Multiphase Flow*, Vol. 29, pp. 1203-1220.

Fujii, T.; Nakazawa, T.; Asano, H.; Yamada, H. and Yoshiyama, T. (1998): Flow characteristics of gas-liquid two-phase annular flow under microgravity (Experimental results utilizing a drop tower). *JSME International Journal.* Vol. 41, pp. 561-567.

Han, H.; Gabriel, K. and Wang, Z. (2005): A new method of entrainment fraction measurement in annular gas-liquid flow in a small diameter vertical tube, submitted to the *Journal of Flow Measurement and Instrumentation*, under review.

Han H.; Zhu, Zh. and Gabriel, K. (2006): A study on the effect of gas flow rate on the wave characteristics in two-phase gas–liquid annular flow. *In Press, Nuclear Engineering and Design*.

Henstock W. H.; Hanratty, T. J. (1976): The Interfacial drag and the Height of the Wall Layer in Annular Flows. *AIChE Journal*, Vol. 22, pp. 990-999.

MacGillivray, R. (2004): *Gravity and gas density effects on annular flow average film thickness and frictional pressure drop*, Master Thesis, University of Saskatchewan, Saskatoon, Saskatchewan, Canada.

MacGillivray, R.; Gabriel, K.S. (2003): A Study of Annular Flow Characteristics in Microgravity and Hypergravity Conditions, *Acta Astronautica,* Vol. 53, pp. 289-297.

MacGillivray, R.; Gabriel, K.S. (2002): Annular Flow Film Characteristics in Variable Gravity, *"Microgravity Transport Processes in Fluid, Thermal, Biological, and Material Sciences," Ann. N.Y. Acad. Sci.*, Vol. 974, pp. 306-315.

Moalem Maron, D.; Brauner, N. (1987): The Role of Interfacial Mobility in Determining the Interfacial Shear Factor in Two-phase Wavy Film Flow. *Int. Com. Heat Mass Transfer*, Vol. 14, pp. 45–55.

Nedderman, R.M.; Shearer, C.J. (1963): The motion and frequency of large disturbance waves in annular two-phase flow of air-water mixtures. *Journal of Chemical*

Engineering Science. Vol. 18, pp. 661-670.

Wang, Zh.; Gabriel, K., (2005): The influence of film structure on the interfacial friction in annular two-phase flow under microgravity and normal gravity conditions. *Microgravity Science and Technology*, XVI – I pp. 264-268.

Wang, Zh.; Gabriel, K. and Manz, D. (2004): The influences of wave height on the interfacial friction in annular gas-liquid flow under normal and microgravity conditions. *International Journal of Multiphase Flow,* Vol. 30, pp.1193-1211.

Wrobel, J. R.; McManus, H. N. (1961): An Analytic Study of Film Depth, Wave Height, and Pressure Drop in Annular Two-phase Flow. *Developments in Mechanics,* Vol. 1, pp. 578–587.

Zhu, Zh., (2004): *A Study of the interfacial features of gas-liquid annular two-phase flow*, Master Thesis, University of Saskatchewan, Saskatoon, Saskatchewan, Canada.

Appendix A: Normal Gravity (1-g) & Microgravity (μ-g) Data

m_l: liquid mass flow rate;

m_g: gas mass flow rate;

FT: average liquid film thickness;

DP/DZ: pressure gradient;

h: wave base thickness (film substrate);

R: wave height (roughness height);

S: wave spacing;

V_w: wave speed;

F: wave frequency.

Notation: in the following tables, the values of m_l and m_g are magnified by 1000 times.

Table 1 : Normal Gravity (1-g) Data.

file	m_{-l} (kg/s)	m_{-g} (kg/s)	FT (mm)	DP/Dz (Pa/m)	h (mm)	R (mm)	S (mm)	Vw (m/s)	F (Hz)
112a	5.4	1.5	0.23	3026	0.181	0.609	66	2.2	16
112b	5.4	1.5	0.24	3035	0.196	0.675	62	2.1	17
111b	5.8	2.0	0.17	4360	0.120	0.438	48	2.7	21
111a	5.8	2.0	0.17	4370	0.124	0.403	47	2.7	22
109a	6.5	1.8	0.19	4407	0.136	0.493	52	2.8	20
109b	6.5	1.8	0.19	4445	0.142	0.452	44	2.6	23
110a	6.6	2.1	0.17	5230	0.126	0.367	38	2.9	27
110b	6.6	2.1	0.17	5240	0.122	0.408	40	2.9	25
108a	6.9	1.7	0.21	4232	0.162	0.551	52	2.5	20
108b	6.9	1.7	0.21	4235	0.163	0.562	51	2.5	20
107a	7.0	1.8	0.2	4540	0.143	0.504	46	2.6	23
107b	7.1	1.8	0.2	4565	0.145	0.489	45	2.7	23
106a	7.2	1.8	0.22	4234	0.153	0.543	49	2.2	21
106b	7.2	1.8	0.22	4241	0.163	0.560	50	2.5	21
105a	7.3	1.0	0.33	2935	0.312	0.845	63	2.0	16
105b	7.3	1.0	0.36	2991	0.323	0.918	72	2.2	14
103a	7.3	2.4	0.16	6114	0.120	0.351	36	3.4	28
104a	7.3	1.6	0.23	4099	0.181	0.581	55	3.0	19
104b	7.3	1.6	0.23	4111	0.183	0.566	49	2.7	21
101a	7.4	1.8	0.23	4577	0.177	0.542	47	2.6	22
101b	7.4	1.8	0.22	4569	0.178	0.507	45	2.7	23
102a	7.4	2.4	0.16	6189	0.119	0.363	35	3.2	29
102b	7.4	2.4	0.16	6177	0.120	0.332	35	3.1	29
103b	7.4	2.4	0.16	6123	0.122	0.359	38	3.4	27
98a	7.6	2.4	0.16	6392	0.117	0.342	33	3.2	31
100a	7.6	2.1	0.19	5632	0.131	0.428	38	3.1	27
100b	7.6	2.1	0.19	5620	0.136	0.423	39	3.1	27
100c	7.6	2.1	0.19	5593	0.130	0.433	41	3.4	25
96a	7.7	3.1	0.14	8014	0.101	0.267	28	3.6	37
96b	7.7	3.1	0.14	7984	0.100	0.275	28	3.6	36
98b	7.7	2.4	0.17	6426	0.118	0.362	34	3.3	30
93a	7.8	2.7	0.15	7176	0.111	0.320	31	3.6	33
93b	7.8	2.7	0.15	7175	0.108	0.310	32	3.4	32
94b	7.8	3.4	0.13	8661	0.092	0.240	27	3.7	38
95a	7.8	2.3	0.17	6036	0.119	0.405	36	3.4	29
97b	7.8	3.4	0.13	8810	0.089	0.244	27	3.8	37

file	m.l (kg/s)	m.g (kg/s)	FT (mm)	DP/Dz (Pa/m)	h (mm)	R (mm)	S (mm)	Vw (m/s)	F (Hz)
91a	7.8	2.9	0.15	7798	0.107	0.296	29	3.5	35
91b	7.8	2.9	0.15	7740	0.109	0.299	30	3.5	34
92b	7.8	1.6	0.24	4477	0.176	0.569	47	2.8	22
94a	7.8	3.4	0.13	8728	0.088	0.248	26	3.8	39
95b	7.8	2.3	0.17	6023	0.126	0.370	36	3.3	29
97a	7.8	3.4	0.13	8757	0.100	0.238	27	3.9	38
99a	7.8	2.7	0.15	7311	0.109	0.313	31	3.8	33
99b	7.8	2.7	0.15	7368	0.114	0.308	30	3.5	34
89b	7.9	2.1	0.2	5827	0.146	0.425	38	3.1	27
92a	7.9	1.6	0.24	4516	0.178	0.603	47	2.6	22
85a	8.0	1.6	0.26	4497	0.205	0.592	47	2.7	22
85b	8.0	1.6	0.26	4486	0.195	0.638	46	2.7	22
89a	8.0	2.1	0.2	5923	0.139	0.440	36	3.4	28
90b	8.0	2.0	0.21	5486	0.152	0.448	38	2.9	27
83a	8.0	3.4	0.14	8872	0.098	0.250	26	3.9	39
83b	8.0	3.4	0.14	8880	0.104	0.246	26	3.7	39
86a	8.0	2.4	0.19	6634	0.134	0.399	36	3.5	29
88a	8.0	2.1	0.2	5874	0.156	0.418	38	3.2	27
88b	8.0	2.1	0.2	5915	0.149	0.423	36	3.0	28
90a	8.0	2.0	0.21	5488	0.159	0.494	39	2.8	26
84a	8.1	3.1	0.15	8209	0.108	0.277	27	3.7	37
84b	8.1	3.1	0.15	8218	0.109	0.277	27	3.7	37
86b	8.1	2.4	0.19	6618	0.135	0.384	34	3.3	30
87a	8.1	2.7	0.17	7436	0.122	0.339	30	3.4	34
87b	8.1	2.7	0.17	7401	0.128	0.318	31	3.6	33
80a	8.2	1.6	0.26	4476	0.192	0.635	50	2.6	21
82a	8.2	2.9	0.16	7874	0.115	0.304	29	3.7	35
82b	8.2	2.9	0.16	7884	0.115	0.301	29	3.8	35
80b	8.2	1.6	0.26	4468	0.204	0.628	48	2.7	21
81a	8.3	3.4	0.13	9285	0.096	0.258	27	4.0	38
75a	8.5	2.5	0.16	7134	0.122	0.340	33	3.4	32
75b	8.5	2.5	0.17	7105	0.116	0.362	33	3.4	31
76b	8.5	2.2	0.18	6410	0.134	0.415	36	3.5	28
77a	8.5	2.4	0.18	6843	0.126	0.387	34	3.4	30
77b	8.5	2.4	0.17	6822	0.122	0.372	33	3.4	32
72a	8.5	2.3	0.19	6497	0.140	0.411	35	3.5	29
76a	8.5	2.2	0.18	6448	0.127	0.399	35	3.3	29
78a	8.5	3.3	0.14	9251	0.094	0.263	27	3.9	38
73a	8.6	2.3	0.18	6519	0.131	0.401	36	3.3	29
73b	8.6	2.3	0.19	6480	0.131	0.429	34	3.3	30
78b	8.6	3.3	0.14	9352	0.100	0.247	26	3.8	40
79a	8.6	2.4	0.18	6967	0.128	0.371	35	3.4	29
72b	8.7	2.3	0.19	6444	0.139	0.431	37	3.5	28
79b	8.7	2.4	0.18	6931	0.129	0.382	35	3.4	29
70b	8.7	2.3	0.19	6595	0.135	0.408	34	3.3	30
71a	8.7	2.2	0.19	6469	0.134	0.407	34	3.2	30
71b	8.7	2.2	0.19	6448	0.144	0.412	35	3.1	29
74a	8.7	2.5	0.16	7292	0.119	0.372	32	3.3	32
74b	8.7	2.5	0.16	7291	0.115	0.343	31	3.3	33
70a	8.8	2.3	0.19	6624	0.133	0.414	36	3.2	29
68a	9.0	1.9	0.22	6138	0.161	0.493	40	2.9	25
68b	9.0	1.9	0.22	6088	0.157	0.493	41	3.1	25
69a	9.0	3.3	0.14	9464	0.106	0.255	24	4.0	42
69b	9.0	3.3	0.14	9469	0.106	0.258	25	3.9	40
66a	9.0	2.5	0.17	8173	0.120	0.366	30	3.8	34
64b	9.1	1.9	0.22	6224	0.153	0.509	41	2.8	25
66b	9.1	2.5	0.17	8163	0.119	0.356	31	3.4	33
67b	9.1	2.1	0.2	6967	0.150	0.416	35	3.2	30
67a	9.2	2.1	0.2	6917	0.150	0.437	38	3.5	27
64a	9.2	1.9	0.22	6232	0.162	0.536	41	3.2	25
65a	9.2	2.2	0.19	7145	0.138	0.406	36	3.2	29
65b	9.3	2.2	0.19	7184	0.144	0.393	35	3.0	29
63a	9.5	2.0	0.22	6541	0.169	0.448	38	3.2	27
63b	9.5	2.0	0.22	6467	0.166	0.503	39	3.1	27
62a	9.6	2.6	0.17	8357	0.119	0.333	29	3.7	35
62b	9.6	2.6	0.17	8320	0.119	0.352	29	3.7	35
61b	10.0	2.3	0.19	7675	0.138	0.418	34	3.2	30
61a	10.0	2.3	0.2	7624	0.144	0.417	34	3.5	30
57b	10.1	2.3	0.2	7952	0.149	0.391	34	3.4	30
57a	10.2	2.3	0.2	8002	0.144	0.415	33	3.5	31
58a	10.2	2.1	0.21	7686	0.147	0.455	34	3.5	30
60a	10.2	2.4	0.19	8367	0.143	0.372	33	3.8	31
56a	10.2	1.3	0.32	4733	0.250	0.769	54	2.9	19
56b	10.2	1.3	0.31	4731	0.236	0.817	59	2.4	17
58b	10.2	2.1	0.21	7684	0.151	0.446	34	3.2	30
59a	10.3	1.8	0.25	6724	0.179	0.552	39	3.0	27
59b	10.3	1.8	0.26	6703	0.185	0.560	41	3.1	25
55a	10.4	1.5	0.29	5208	0.227	0.675	47	3.1	22
55b	10.4	1.5	0.29	5214	0.228	0.666	45	3.0	23
54a	10.5	2.3	0.21	8215	0.143	0.432	33	3.6	31
54b	10.6	2.3	0.21	8218	0.153	0.411	32	3.5	32
50a	10.7	2.6	0.18	9397	0.120	0.363	28	3.7	36
50b	10.7	2.6	0.17	9483	0.120	0.356	28	3.7	36
53a	10.7	2.1	0.21	7845	0.148	0.461	34	3.6	30
53b	10.7	2.1	0.21	7900	0.146	0.441	34	3.5	30
52a	10.7	2.0	0.23	7249	0.170	0.495	37	3.2	27
52b	10.7	2.0	0.23	7222	0.172	0.532	39	3.3	26
51a	10.8	1.8	0.24	6777	0.166	0.577	40	3.0	25
51b	10.8	1.8	0.24	6799	0.177	0.573	40	3.0	25
45a	11.0	2.0	0.24	7567	0.174	0.494	35	3.1	29
47a	11.0	2.6	0.19	9458	0.133	0.363	30	3.8	34
48a	11.0	1.3	0.36	5067	0.278	0.803	51	2.7	20
48b	11.0	1.3	0.35	5022	0.282	0.870	53	2.7	19
49a	11.0	2.2	0.21	8450	0.153	0.469	35	3.6	29
49b	11.0	2.2	0.21	8383	0.148	0.450	32	3.4	32
45b	11.1	2.0	0.24	7588	0.173	0.505	36	3.3	29
47b	11.1	2.6	0.19	9459	0.129	0.391	30	3.7	34
46a	11.2	2.0	0.25	7507	0.188	0.516	37	3.5	27
46b	11.2	2.0	0.25	7497	0.182	0.502	35	3.2	29
43a	11.3	2.0	0.26	7382	0.192	0.527	37	3.4	27
44a	11.3	2.3	0.23	8547	0.163	0.439	32	3.8	32
42a	11.4	2.3	0.23	8306	0.160	0.498	32	3.4	32
42b	11.4	2.3	0.23	8366	0.164	0.468	32	3.3	32
43b	11.6	2.0	0.25	7338	0.179	0.550	37	3.4	27
44b	11.6	2.3	0.22	8370	0.169	0.443	35	3.6	29
41a	11.7	1.6	0.31	6403	0.235	0.679	43	3.3	24
41b	11.7	1.6	0.31	6405	0.234	0.698	42	3.4	24
40a	11.7	1.8	0.28	7219	0.212	0.593	38	3.1	27
40b	11.7	1.8	0.28	7197	0.213	0.593	38	3.5	27

Table 2 : Microgravity (μ-g) Data.

file	$m_{.l}$ (kg/s)	$m_{.g}$ (kg/s)	FT (mm)	DP/Dz (Pa/m)	h (mm)	R (mm)	S (mm)	Vw (m/s)	F (Hz)
112a	5.4	1.5	0.23	3026	0.181	0.609	66	2.2	16
112b	5.4	1.5	0.24	3035	0.196	0.675	62	2.1	17
111b	5.8	2.0	0.17	4360	0.120	0.438	48	2.7	21
111a	5.8	2.0	0.17	4370	0.124	0.403	47	2.7	22
109a	6.5	1.8	0.19	4407	0.136	0.493	52	2.8	20
109b	6.5	1.8	0.19	4445	0.142	0.452	44	2.6	23
110a	6.6	2.1	0.17	5230	0.126	0.367	38	2.9	27
110b	6.6	2.1	0.17	5240	0.122	0.408	40	2.9	25
108a	6.9	1.7	0.21	4232	0.162	0.551	52	2.5	20
108b	6.9	1.7	0.21	4235	0.163	0.562	51	2.5	20
107a	7.0	1.8	0.2	4540	0.143	0.504	46	2.6	23
107b	7.1	1.8	0.2	4565	0.145	0.489	45	2.7	23
106a	7.2	1.8	0.22	4234	0.153	0.543	49	2.2	21
106b	7.2	1.8	0.22	4241	0.163	0.560	50	2.5	21
105a	7.3	1.0	0.33	2935	0.312	0.845	63	2.0	16
105b	7.3	1.0	0.36	2991	0.323	0.918	72	2.2	14
103a	7.3	2.4	0.16	6114	0.120	0.351	36	3.4	28
104a	7.3	1.6	0.23	4099	0.181	0.581	55	3.0	19
104b	7.3	1.6	0.23	4111	0.183	0.566	49	2.7	21
101a	7.4	1.8	0.23	4577	0.177	0.542	47	2.6	22
101b	7.4	1.8	0.22	4569	0.178	0.507	45	2.7	23
102a	7.4	2.4	0.16	6189	0.119	0.363	35	3.2	29
102b	7.4	2.4	0.16	6177	0.120	0.332	35	3.1	29
103b	7.4	2.4	0.16	6123	0.122	0.359	38	3.4	27
98a	7.6	2.4	0.16	6392	0.117	0.342	33	3.2	31
100a	7.6	2.1	0.19	5632	0.131	0.428	38	3.1	27
100b	7.6	2.1	0.19	5620	0.136	0.423	39	3.1	27
100c	7.6	2.1	0.19	5593	0.130	0.433	41	3.4	25
96a	7.7	3.1	0.14	8014	0.101	0.267	28	3.6	37
96b	7.7	3.1	0.14	7984	0.100	0.275	28	3.6	36
98b	7.7	2.4	0.17	6426	0.118	0.362	34	3.3	30
93a	7.8	2.7	0.15	7176	0.111	0.320	31	3.6	33
93b	7.8	2.7	0.15	7175	0.108	0.310	32	3.4	32
94b	7.8	3.4	0.13	8661	0.092	0.240	27	3.7	38
95a	7.8	2.3	0.17	6036	0.119	0.405	36	3.4	29
97b	7.8	3.4	0.13	8810	0.089	0.244	27	3.8	37